GASP - XVII. H I imaging of the jellyfish galaxy JO206

Ramatsoku, M.; Serra, P.; Poggianti, B. M.; Moretti, A.; Gullieuszik, M.; Bettoni, D.; Deb, T.; Fritz, J.; van Gorkom, J. H.; Jaffé, Y. L.

IMPORTANT NOTE: You are advised to consult the publisher's version (publisher's PDF) if you wish to cite from it. Please check the document version below.

Document Version
Publisher's PDF, also known as Version of record

[Link to publication in University of Groningen/UMCG research database](#)

GASP – XVII. H I imaging of the jellyfish galaxy JO206: gas stripping and enhanced star formation

M. Ramatsoku [1]★ P. Serra,[1]★ B. M Poggianti,[2] A. Moretti [2] M. Gullieuszik,[2]
D. Bettoni,[2] T. Deb,[3] J. Fritz [4] J. H. van Gorkom,[5] Y. L. Jaffé [6] S. Tonnesen,[7]
M. A. W Verheijen,[3,8] B. Vulcani [2] B. Hugo,[9,10] G. I. G. Józsa,[9,10,11] F. M. Maccagni,[1]
S. Makhathini,[9,10] A. Ramaila,[9,10] O. Smirnov[9,10] and K. Thorat[9,10]

[1]*INAF- Osservatorio Astronomico di Cagliari, Via della Scienza 5, I-09047 Selargius (CA), Italy*
[2]*INAF- Osservatorio Astronomico di Padova, Vicolo dell'Osservatorio 5, I-35122 Padova, Italy*
[3]*Kapteyn Astronomical Institute, University of Groningen, Landleven 12, NL-9747 AV Groningen, the Netherlands*
[4]*Instituto de Radioastronomia y Astrofisica, UNAM, Campus Morelia, A.P. 3-72, C.P. 58089, Mexico*
[5]*Department of Astronomy, Columbia University, Mail Code 5246, 550 W 120th Street, New York, NY 10027, USA*
[6]*Instituto de Física y Astronomía, Facultad de Ciencias, Universidad de Valparaíso, Avda. Gran Bretana 1111 Valparaíso, Chile*
[7]*Center for Computational Astrophysics, Flatiron Institute, 162 5th Ave, New York, NY 10010, USA*
[8]*National Centre for Radio Astrophysics, Tata Institute of Fundamental Research, Postbag 3, Ganeshkhind, Pune 411 007, India*
[9]*South African Radio Astronomy Observatory, 2 Fir Street, Black River Park, Observatory 7925, South Africa*
[10]*Department of Physics & Electronics, Rhodes University, Makhanda 6139, South Africa*
[11]*Argelander-Institut für Astronomie, Auf dem Hügel 71, D-53121 Bonn, Germany*

ABSTRACT

We present VLA H I observations of JO206, a prototypical ram-pressure-stripped galaxy in the GASP sample. This massive galaxy ($M_* = 8.5 \times 10^{10}$ M$_\odot$) is located at a redshift of $z = 0.0513$, near the centre of the low-mass galaxy cluster, IIZw108 ($\sigma \sim 575$ km s^{-1}). JO206 is characterized by a long tail (≥ 90 kpc) of ionized gas stripped away by ram pressure. We find a similarly long H I tail in the same direction as the ionized gas tail and measure a total H I mass of 3.2×10^9 M$_\odot$. This is about half the expected H I mass given the stellar mass and surface density of JO206. A total of 1.8×10^9 M$_\odot$ (60 per cent) of the detected H I is in the gas-stripped tail. An analysis of the star formation rate shows that the galaxy is forming more stars compared to galaxies with the same stellar and H I mass. On average we find an H I gas depletion time of ~ 0.5 Gyr which is about four times shorter than that of 'normal' spiral galaxies. We performed a spatially resolved analysis of the relation between star formation rate density and gas density in the disc and tail of the galaxy at the resolution of our H I data. The star formation efficiency of the disc is about 10 times higher than that of the tail at fixed H I surface densities. Both the inner and outer parts of JO206 show an enhanced star formation compared to regions of similar H I surface density in field galaxies. The enhanced star formation is due to ram-pressure stripping during the galaxy's first infall into the cluster.

Key words: galaxies: clusters: intracluster medium.

1 INTRODUCTION

One of the fundamental processes that affects the evolution of galaxies is their star formation activity. Galaxy surveys have shown that the star formation activity decreases with redshift such that galaxies with higher star formation rates (SFRs) are more abundant at higher redshifts (Noeske et al. 2007; Madau & Dickinson 2014;

van der Wel et al. 2014). The gradually decreasing SFR has resulted in passive or 'quenched' galaxies and the evolution of galaxies from late- to early-type (Dressler et al. 1997; Postman et al. 2005; Smith et al. 2005). Since gas is the main ingredient in star formation it is crucial to understand how galaxies acquire and lose their gas (Larson 1972; Dekel & Birnboim 2006; Silk & Mamon 2012). Internal and external processes are known to be involved in the gas acquisition or loss. Of the internal processes, the basic is the cooling of the hot gas in the dark matter haloes of galaxies. As the gas cools it drops down into the interstellar medium (ISM) of the

★ E-mail: mpati.ramatsoku@inaf.it (MR); paolo.serra@inaf.it (PS)

galactic discs (White & Frenk 1991; King & Pounds 2015). This gas sometimes gets mechanically displaced or ionized thus affecting the star formation activity.

The environment plays a crucial role in creating the external processes which affect the galaxy star formation activity. For instance, galaxies in densely populated environments such as galaxy clusters have been observed to have their star formation dampened or quenched more efficiently than their counterparts in the field (Dressler 1980; Cooper et al. 2007; George et al. 2011; Whitaker et al. 2012; Nantais et al. 2017; Foltz et al. 2018). This is often due to gas removal mechanisms that take place in these dense environments (Boselli & Gavazzi 2006; De Lucia 2011).

In processes such as mergers gas is removed from a galaxy as it becomes gravitationally detached during the collision (Toomre & Toomre 1972; Walker, Mihos & Hernquist 1996). Depending on the geometry and total angular momentum of the system it is possible for the perturbed gas to be funnelled to the nuclear regions where it sometimes gets consumed by star formation or contributes to fuelling an active galactic nuclei (AGNs) (Baldry et al. 2004; Balogh et al. 2009). In processes such as harassment the gas and stellar distributions get perturbed. In instances of this process the majority of the gas clouds will be affected and the galaxy will undergo an abrupt burst of star formation which consumes all of the fuel for new stars (Moore et al. 1996; Duc & Bournaud 2008; Smith et al. 2015). In less severe harassment cases only the diffuse gaseous halo is perturbed, effectively stopping the gas from cooling and condensing thus quenching star formation in a galaxy (Dressler et al. 2013; Cattaneo 2015; Peng, Maiolino & Cochrane 2015; Jaffé et al. 2016).

Other mechanisms only affect the gas component of galaxies. One of the most well known is ram-pressure stripping. This particular process has often been observed in rich galaxy clusters containing hot X-ray-emitting gas which forms the intracluster medium (ICM). As a galaxy falls into the cluster core it passes through this ICM which exerts hydrodynamical pressure on the galaxy. If the ICM pressure is sufficiently high it can overpower the gravitational force keeping the gas bound to the galaxy, effectively stripping the galaxy of its star-forming fuel (Gunn & Gott 1972; Moran et al. 2007; Porter et al. 2008; Dressler et al. 2013; Jaffé et al. 2015).

Extreme examples of ram-pressure stripping are seen in the so-called 'jellyfish' galaxies. These objects are so named because they show one-sided tails seemingly stripped from the main galaxy body (Yagi et al. 2007; Smith et al. 2010; Fumagalli et al. 2014). Knots of recent star formation are often observed in these tails.

The GAs Stripping Phenomena survey (GASP; Poggianti et al. 2017b) was conducted with the aim of identifying and collecting a statistically significant sample of these galaxies in nearby clusters ($z = 0.04$–0.07) from the WIde-field Nearby Galaxy-cluster Survey (WINGS; Fasano et al. 2006). Within the context of the GASP sample, a galaxy is considered a jellyfish if its Hα tail is at least as long as its stellar disc diameter. Using the MUSE Integral Field spectrograph on the VLT, 94 optically selected stripping candidates (Poggianti et al. 2016) were observed. This sample of galaxies has a wide range of jellyfish morphological asymmetries and masses in varying environments. The focus of the survey is to study all phases of the gas and stellar populations in these galaxies, and to quantify the amount of star formation activity during the process of gas stripping.

One of the primary ways to examine the star formation activity of a galaxy in relation to gas stripping is by studying its neutral gas (H I) content. A total of about 25 per cent of the ISM of a typical spiral galaxy is composed of H I (Boulares & Cox 1990). It is

usually distributed out to large radii of about 1.5–1.8 optical R_{25} radii (Broeils & Rhee 1997; Walter et al. 2008), where the gravitational force binding it to the host galaxy is weaker, thus making it easy to remove, particularly in cluster and group environments (Haynes, Giovanelli & Chincarini 1984; Bravo-Alfaro et al. 1997; Gavazzi et al. 2008). This H I property makes it an excellent tracer of tidal or hydrodynamical gas removal processes (Chung et al. 2009; Kapferer et al. 2009; Abramson et al. 2011; Jaffé et al. 2015; Yoon et al. 2017).

H I observations of spiral galaxies in clusters such as Virgo (Chung et al. 2009) have shown that galaxies located at low cluster-centric distances ($\leq$0.5 Mpc) tend to have smaller H I discs than the stellar disc (Chung et al. 2007). These results are often explained by ram-pressure stripping. In the Virgo cluster, the VLA Imaging of Virgo in Atomic gas survey (VIVA; Chung et al. 2009) found that seven spirals galaxies out of a sample of 50 had long H I tails extending well beyond the optical disc. All of these tails point away from the centre of the cluster (M 87). H I tails were also reported in the Coma cluster through H I-imaging observations of 19 brightest galaxies in the cluster (Bravo-Alfaro et al. 2000). In addition to asymmetries in H I, tracers of young stars in the form of Hα and UV emission were also found to be a typical feature of ram-pressure-stripped galaxies (Cortese et al. 2006; Sun, Donahue & Voit 2007; Kenney et al. 2008; Yagi et al. 2010; Fumagalli et al. 2014; Boselli et al. 2016; Fossati et al. 2016). In rare cases tails are observed in radio continuum and X-rays as well (Gavazzi et al. 1995; Vollmer et al. 2004; Sun & Vikhlinin 2005; Sun et al. 2010).

There is a large body of simulation-based work studying ram-pressure stripping (e.g. Abadi, Moore & Bower 1999; Quilis, Moore & Bower 2000; Schulz & Struck 2001; Vollmer et al. 2001, 2003, 2006, 2008, 2009, 2012; Roediger & Hensler 2005; Roediger & Brüggen 2006, 2007, 2008; Jáchym et al. 2007, 2009; Kronberger et al. 2008; Kapferer et al. 2009; Tonnesen & Bryan 2009, 2010) some of which has focused on H I. For example, Vollmer et al. (2003, 2005, 2006, 2008) uses *N*-body simulations and models of orbiting galaxies in the Virgo cluster to carefully model both the remaining and stripped H I gas. Through comparisons with observations, the authors interpret the stripping and interaction history of several galaxies in the cluster (see also Merluzzi et al. 2013, 2016; Gullieuszik et al. 2017 for similar comparisons with Hα-emitting gas). The H I velocity and spatial information of ram-pressure-stripped galaxies may allow for tight constraints on the history of satellite galaxies.

Simulations have also been used to make more general predictions about ram-pressure stripping. For example, Quilis et al. (2000) argued that observed holes in the H I gas disc allowed for fast, complete ram-pressure stripping. Using smooth gas density profiles, Roediger & Brüggen (2007) find that the amount of gas stripped is well matched by the analytical arguments of Gunn & Gott (1972), that gas will be removed at radii where ram pressure overcomes the restoring force of the disc. Using simulations that included radiative cooling, Tonnesen & Bryan (2009) also found that the total gas removed from galaxies was similar to that predicted using the Gunn & Gott (1972) prescription, but stripping acted much more quickly. The ICM wind removed low-density gas from a range of radii, leaving behind dense clouds (also see Schulz & Struck 2001). Tonnesen & Bryan (2010) focused on the stripped tail of gas, and found that radiative cooling allowed for long, narrow tails of stripped gas with high surface density H I, as observed in some ram-pressure-stripped galaxies.

To fully understand the effect of ram-pressure stripping on the GASP galaxy sample it is imperative to examine the H I content and distribution of these galaxies.

In this paper we focus on the H I gas phase of a quintessential 'jellyfish' galaxy in the GASP sample, namely JO206 (α_{J2000}, δ_{J2000}, z = 1:13:47.4, + 02:28:35.5, = 0.0513; Gullieuszik et al. 2015; Moretti et al. 2017). This massive galaxy is located near the centre of a low-mass galaxy cluster and exhibits a long tail ($\geq$90 kpc) of ionized gas stripped away by ram pressure (Poggianti et al. 2017b). Our aim is to investigate the impact of this stripping event on the neutral ISM of JO206, and to understand the relationship between this neutral ISM and the star formation activity traced by the ionized gas both within and outside the galaxy disc.

In Section 2 we give an overview of the JO206 properties and the environment in which it resides. A further brief discussion of the galaxy's currently available multiwavelength data is given in the same section. H I observations conducted with the VLA and data processing are outlined in Section 3. We provide an analysis of the H I results in Section 4. In Section 5 we assess and discuss the relation between the H I gas and star formation activity in the galaxy. The analyses and discussions are summarized in Section 6.

Throughout this paper, we adopt a Chabrier (2003) initial mass function (IMF) and assume a Λ cold dark matter cosmology with $\Omega_M = 0.3$, $\Lambda_\Omega = 0.7$, and a Hubble constant, $H_0 = 70$ km s^{-1} Mpc^{-1}.

2 JO206 PROPERTIES AND ENVIRONMENT

The JO206 galaxy is massive with a total stellar mass of 8.5×10^{10} M$_\odot$ and hosts an AGN (Poggianti et al. 2017a). It is a member of a poor galaxy cluster known as IIZw108 ($z = 0.04889$; Biviano et al. 2017) in the WINGS/OmegaWINGS sample (Fasano et al. 2006; Cava et al. 2009; Varela et al. 2009; Gullieuszik et al. 2015; Moretti et al. 2017). The host cluster has a velocity dispersion and an X-ray luminosity of $\sigma_{cl} \sim 575 \pm 33$ km s^{-1} (Biviano et al. 2017) and $L_X = 1.09 \times 10^{44}$ erg s^{-1} (0.1–2.4 keV; Smith et al. 2004), respectively, and a dynamical mass $M_{200} \sim 2 \times 10^{14}$ M$_\odot$ (Biviano et al. 2017).

The galaxy has been assigned the highest jellyfish morphological classification of JClass = 5 since it exhibits the most recognizable tail of debris material that is apparently stripped from the galaxy main body (Poggianti et al. 2016). The stripped tail of material is thought to be the result of ram-pressure stripping due to the ICM of the IIZw108 galaxy cluster. This claim has been supported by the galaxy location close to the cluster centre at the projected radial distance of $\sim$350 kpc (see Fig. 1) and its high line-of-sight velocity of $1.5\sigma_{cl}$ relative to the cluster's mean systemic velocity and centre.

2.1 Estimated fraction of stripped gas

Analyses of the dynamics of IIZw108 have shown that JO206 does not belong to any substructure and appears to be an isolated galaxy falling into the cluster (Poggianti et al. 2017b). We recalculated the fraction of stripped gas presented in Poggianti et al. (2017b) using both the truncation radius in Hα and the location of JO206 in projected position versus velocity phase space, following the method presented in Jaffe et al. (2018), and using the beta model for IIZw108's ICM presented in Reiprich (2001) (rather than the Virgo cluster). An in-depth description and detailed calculation of the ram-pressure stripping strength of the cluster are discussed and presented in section 7.6 in Poggianti et al. (2017b); see also Jaffe et al. (2018). In short, we assume instantaneous gas stripping (following Gunn & Gott 1972) from a pure exponential disc falling into a homogeneous and symmetrical ICM. In the phase-space method we compare the intensity of ram pressure at the projected position and velocity of the galaxy within the cluster ($P_{ram} \simeq 5.3 \times 10^{-13}$ N m^2) with the
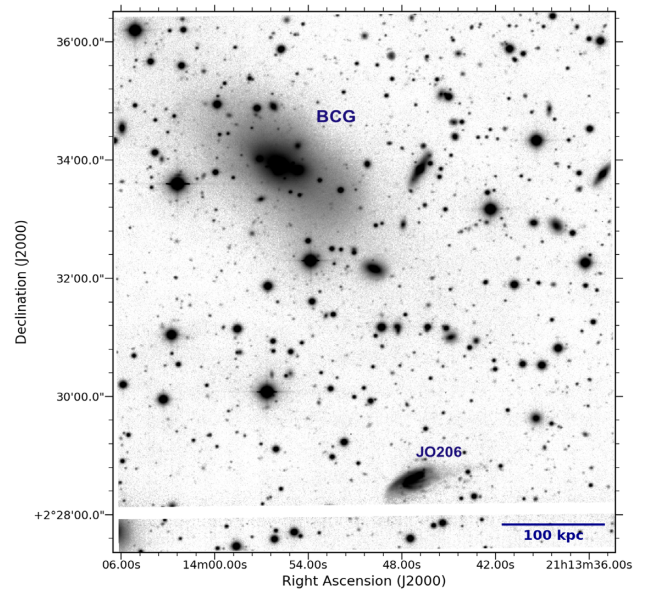

Figure 1. A *V*-band image of the central region of the IIZw108 galaxy cluster from WINGS. The JO206 galaxy and the BCG that defines the centre of the cluster are labelled as such. They are separated by $\sim$350 kpc at the distance of the cluster of $\sim$208 Mpc.

restoring force of the galaxy (Π_{gal} which decreases with radial distance from the centre of the galaxy). Stripping will occur when $P_{ram} > \Pi_{gal}$. Using the galaxy radius where the stripping condition is found, we then estimate the amount of gas lost due to stripping to be $\sim$70 per cent (assuming an initial gas fraction of 10 per cent with an extent 1.7 larger than the stellar disc). As this method has a lot of uncertainties (see caveats section in Jaffe et al. 2018), we also estimated the amount of gas lost purely from the extent of Hα relative to the size of the disc, and get a lower fraction of stripped gas ($\sim$40 per cent). We therefore conclude that J0206 has lost between $\sim$40 per cent and $\sim$70 per cent of its total gas mass due to ram-pressure stripping.

2.2 Star formation

Regardless of this gas loss, ram-pressure stripping is believed to have resulted in a burst of new stars. The galaxy has a reported SFR of 5.6 M$_\odot$ yr^{-1} determined from Hα and excluding the contribution of the central AGN (Poggianti et al. 2017b). All the SFRs reported in this paper are computed from the MUSE Hα luminosity corrected for dust and stellar absorption using equation (1) in Poggianti et al. (2017b), with the dust correction being estimated from the Balmer decrements measured from the MUSE spectra.[1] The JO206 stellar spatial distribution shows that the oldest stars with ages >0.6 Gyr are only found within the main galaxy body. The stripped tail on the other hand comprises young stars that would have started forming $\sim$0.5 Gyr ago or less (see fig. 16 by Poggianti et al. 2017b).

2.3 MUSE and APEX observations

The galaxy was first observed with the MUSE IF spectrograph in 2017 August. Observations were carried out using two pointings

---

[1]Note that star formation rates are derived adopting a Chabrier (2003) IMF and a Cardelli, Clayton & Mathis (1989) extinction curve.
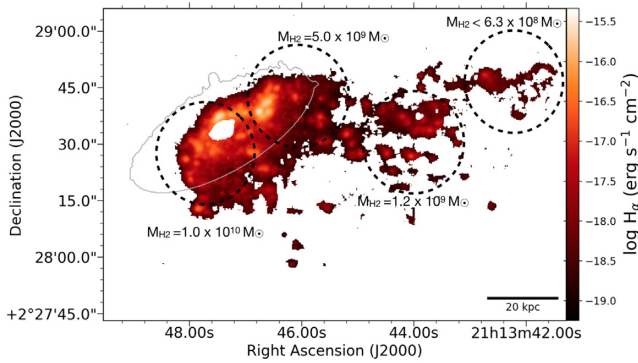
Figure 2. The MUSE Hα map (Poggianti et al. 2017b) with the APEX pointings overlaid (Moretti et al. 2018). The contour delineates the main galaxy body (see the text for a description) and the location of the AGN is represented by the white patch in the middle of the galaxy's main body. The approximate full width at half-maximum (FWHM) of the APEX beam are shown by the black dashed circles with the measured H$_2$ mass indicated for each region.

which covered both the galaxy body and tail. The exposure time for each of the pointing was 2700 s with a seeing of 1 and 1.2 arcsec. A detailed description of these observations and the data reduction is given in Poggianti et al. (2017b). That paper also presents a detailed analysis of the MUSE observations that show the Hα tentacles of the stripped debris material. We have also obtained recent MUSE observations covering the southern part of the galaxy. These observations were conducted to investigate a possible southern Hα tail which was hinted by the H I observations (see Section 4). Throughout this paper we use this recent Hα map which includes the southern region of the galaxy. The full details of these additional observations and data reduction are given in Appendix A.

The tentacle of debris material apparent in the optical image (see Fig. 1) becomes much clearer in the Hα MUSE map shown in Fig. 2. In this map the main galaxy body (i.e. the stellar disc) is outlined by the grey contour. The contour was defined from the from the MUSE image using the continuum at the Hα wavelength, with the isophote fit at surface brightness of 1σ above the average sky background level (Gullieuszik et al., in preparation). The image shows a tail of Hα emission extending over 90 kpc to the west of the main galaxy body characterized by regions of clumpy and diffuse Hα emission.

In addition to the optical and Hα data, the molecular gas phase of JO206 has also been observed with the Atacama Pathfinder Experiment (APEX; Güsten et al. 2006) telescope. These observations were conducted in 2016 December and 2017 April–July. The ^{12}CO(2-1) transition was observed in four locations of the galaxy shown in Fig. 2. The APEX pointings covered the main galaxy body and the tail. The details of these observations, the data reduction and analysis are fully described in Moretti et al. (2018).

The APEX data revealed clear CO line detections in the central location of the main galaxy body where the AGN is located, and where the tail of the galaxy begins at about 30 kpc west of the centre. In these two locations the CO emission coincides with the bright Hα emissions. However, no secure CO detections coinciding with the Hα peaks over 40 kpc away from the galaxy disc were found (Moretti et al. 2018).

All these data have provided an excellent laboratory comprising the ionized and molecular gas and stars within the galaxy disc and its tails. This is all due to the MUSE large field of view which has

Table 1. A summary of the H I observations.

Properties	JO205-206
Pointing centre:	
α (J2000)	$21^h 13^m 46^s.7$
δ (J2000)	$02° 21' 20''.0$
Central velocity (radio, barycentric)	$15\,388$ km s^{-1}
Calibrators:	
Gain	J2130+0502
Flux and bandpass	3C48
On-source integration	16 h
Observation dates	2017 July and August
Sensitivity (r.m.s per channel)	0.3 mJy beam^{-1}
Channel width	6.56 km s^{-1}
Beam (FWHM) (P.A)	26 arcsec × 18 arcsec (159°)

allowed for the examination of the galaxy's main body, its tails, and surroundings.

As discussed above, this jellyfish galaxy is experiencing ram-pressure stripping while falling into the cluster for the first time. Because of its first infall status it still contains a lot of its gas, thus the recent star formation along its tail. Given the close relation between star formation and cold gas, one of the crucial missing components to complete the picture of the ram-pressure stripping effect on the star formation activity of this galaxy was its neutral gas (H I) phase.

3 H I OBSERVATIONS AND DATA PROCESSING

H I observations were conducted with the Very Large Array (VLA; Perley et al. 2009) in its C-array configuration between 2017 July and 2017 August. We chose this configuration to achieve a spatial resolution of ∼15 arcsec which would allow the detection of the low surface brightness H I particularly in the galaxy tail. The galaxy field was observed for a total on-source integration time of 2 × 8 h with an additional 4 h for the bandpass and phase calibrators. Data were obtained over the frequency range of 1335–1367 MHz, centred at 1351 MHz. This covered a total effective bandwidth of 32 MHz with 1024 channels that are 31.25 kHz wide (6.56 km s^{-1} for H I at $z = 0$). With this configuration both the JO206 galaxy and the IIZw108 galaxy cluster as a whole were covered by the observed pointing. A summary of the observational parameters is given in Table 1.

The uv-data were processed following standard procedures using a new data reduction pipeline developed at SARAO[2] and INAF-Cagliari[3] to process mainly data from upcoming MeerKAT[4] surveys. It also works on data from other interferometers such as the VLA, GMRT, etc. This pipeline comprises various radio data reduction tools and packages such as CASA (McMullin et al. 2007), AOFLAGGER (Offringa et al. 2010), SOFIA (Serra et al. 2015), WSCLEAN (Offringa et al. 2014) among many others.

Within this pipeline CASA tasks were used to determine and apply antenna-based complex bandpass (independent of time) and gains (independent of frequency). Our calibrators were 3C 48 (for bandpass and flux scale) and J2130+0502 (for the gains). Strong radio frequency interference affecting the calibrators and the target source was flagged using AOFLAGGER. Continuum source subtraction was performed in the uv-plane using the *uvcontsub*

task in CASA. This was done in two steps, first we made a linear fit to the uv-data using all the channels. The flagged, calibrated, and continuum-subtracted uv-data were Fourier transformed into an image cube with WSCLEAN. We then used SOFIA to identify channels with H I-line emission, and repeated the continuum subtraction excluding those channels from the fit. A third-order polynomial fit was necessary to subtract all continuum emission satisfactorily. The improved continuum-subtracted uv-data were the re-Fourier transformed into a final H I cube using a pixel size of 5 arcsec, a field of view of 0.7 deg², and natural weighting with Briggs robustness parameter = 2 to optimize surface-brightness sensitivity. The resulting cube has an rms noise level of $\sigma \approx 0.3$ mJy beam^{-1} per channel. To eliminate the sidelobes of the synthesized beam we used WSCLEAN and SOFIA iteratively to define 3D clean regions in the H I cube and clean within them down to 0.5σ. The restoring Gaussian PSF has FWHM of 18 and 26 arcsec along minor and major axis ($\sim$18 kpc × 26 kpc), respectively (PA = 159°). Our observational set-up allowed us to reach the H I column density sensitivity of 3×10^{19} atoms cm^{-2} assuming a line width of 30 km s^{-1} at the 3σ noise level. To obtain an H I cube at higher angular resolution we repeated the imaging steps with a range of values of the Briggs robust parameter. In Section 4 we will also show results obtained with robust = 0, which gave the highest obtainable angular resolution of 14 arcsec × 13 arcsec, a slightly higher noise level of $\sim$0.4 mJy beam^{-1} and a column density sensitivity of 9×10^{19} atoms cm^{-2} at 3σ and for a 30 km s^{-1} line width.

H I column density and mass: The H I-line emission in units of Jy beam^{-1} of the galaxy of interest (JO206) was extracted from the image cube using SOFIA. We then converted the H I map units from Jy beam^{-1} km s^{-1} to column densities in atoms cm^{-2} using

$$N_{H I} = 1.104 \times 10^{21} \int \frac{S_v}{B_{maj} B_{min}} \, dv \, , \qquad (1)$$

where S_v is the flux density in mJy beam^{-1}, B_{maj} and B_{min} are the major and minor axes of the beam in arcsec, and dv is the channel width in km s^{-1}.

We derived the H I mass ($M_\odot$) using the formulation

$$M_{H I} = 2.36 \times 10^5 D^2 \int S_v dv \, , \qquad (2)$$

where $\int S_v dv$ is the total integrated flux expressed in Jy km s^{-1} and D is the distance to the galaxy in Mpc.

4 RESULTS

We calculated the total H I mass for JO206 using equation (2) with $\int S_v dv = 0.27$ Jy km s^{-1} as derived from the H I map. We assume that the galaxy is at the same distance as the cluster, D = 208 Mpc. With these values we measured a total H I mass, $M_{H I} = 3.2 \times 10^9$ M$_\odot$.

4.1 H I morphology

Fig. 3 shows the H I column density distribution overlaid on an optical *V*-band image from WINGS. For completeness we also show the contours extracted from an H I cube with an FWHM beam size of 14 arcsec × 13 arcsec. These are plotted to highlight locations with high-density H I. When compared to the optical image, the H I distribution appears compressed and truncated within the stellar disc on the east side. On the west side it extends well beyond the stellar disc. This extension coincides with the $\sim$90 kpc Hα tail shown in Fig. 2. Furthermore, the peak H I surface brightness is 10 arcsec

($\sim$10 kpc) offset from the optical centre of the galaxy. This offset is in the same direction as the H I and Hα tails. We have inspected the optical image (Fig. 1) and the entire H I cube over a spatial area of 0.7 deg² and the radial velocity range of $v_{rad} \sim 12\,000$–$17\,000$ km s^{-1}, we found no obvious and potentially interacting cluster member(s) near and around JO206 nor along its H I tail. Thus, the observed H I morphology is consistent with the effect of ram-pressure gas stripping by the ICM of its host galaxy cluster.

4.2 H I deficiency

As shown in the preceding section, the H I distribution of JO206 appears to have been affected by ram pressure resulting in a long H I tail. In this section we examine how much of the galaxy's H I content has been displaced or removed by ram pressure. This is done by comparing the current, measured H I fraction ($M_{H I}/M_*$) of JO206 with the expected H I fraction based on known H I scaling relations derived from large samples. We use relations by Brown et al. (2015) obtained using ALFALFA data. These relations were chosen because they are based on the H I spectral stacking technique. They are therefore expected to be more robust since they are not biased towards H I-rich, detected galaxies (Fabello et al. 2012; Huang et al. 2012; Brown et al. 2015). Here we assess the observed H I gas fraction as a function of stellar mass and surface density.

The stellar surface density of JO206 was derived using

$$\mu_* = \frac{M_*}{2\pi R_{50}^2} \, , \qquad (3)$$

where M_* is the stellar mass (see Section 2) and R_{50} is the Petrosian radius containing 50 per cent of the flux level. We find a stellar mass surface density, $\mu_* = 4.2 \times 10^8$ M$_\odot$ kpc^{-2}. Note that the scaling relations by Brown et al. (2015) are based on z-band R_{50} radii while for JO206 we have used the K-band R_{50} radius from Valentinuzzi et al. (2009); z-band parameters are not available for this galaxy. Based on the SDSS (DR15; Aguado et al. 2019), 2MASS (Skrutskie et al. 2006), and parameters of galaxies in the xGASS sample (Catinella et al. 2018), we find that z-band R_{50} radii are systematically smaller than the K-band ones by a factor 1.15. This results in a systematic increase of μ_* by a factor 1.32, which is small compared to the uncertainty on μ_* associated with the M_* in equation (3), and furthermore, does not change the conclusions of our comparison between JO206 and a control sample discussed below.

Fig. 4 shows the relation of the H I fraction as a function of stellar mass for galaxies in which μ_* is the same as that of JO206 within a factor of 4. This factor is much larger than the aforementioned systematic error on μ_* caused by using the K-band rather than z-band R_{50} radius. JO206 is indicated by the blue asterisk on this relation. A comparison of the measured stellar surface density of JO206 with its counterparts in the range $\log \mu_* = 8.0$ to 9.2, places it about 0.3 dex below the average H I fraction. Based on this scaling relation the galaxy appears to be H I deficient and missing about 50 per cent of its expected H I gas mass compared to galaxies with the same M_* and μ_*. This is consistent with the gas loss estimated as described Section 2.1.

4.3 H I displacement

Having established that the galaxy has lost about 50 per cent of its initial H I, Fig. 3 shows that most of the remaining H I is not distributed on a settled disc. In this section we aim to quantify the displacement relative to the galaxy disc in order to establish how much of the H I is at larger radii than expected for an H I disc with
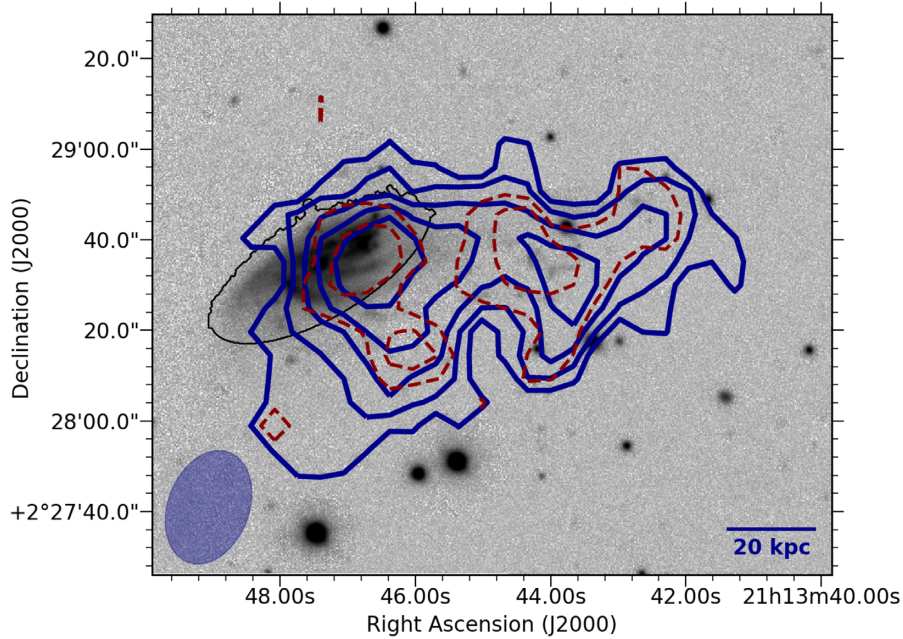
Figure 3. The VLA H I column density contours overlaid on the *V*-band image of JO206 from WINGS (*V*-band image from Moretti et al. 2014). The blue contour drawn at column densities of 3, 6, 9, ... × 10^{19} atoms cm^{-2} are from an image with FWHM beam size of 26 arcsec × 18 arcsec indicated by the blue ellipse. The red contours are column densities levels of 10, 20, ... × 10^{19} atoms cm^{-2} from an image with FWHM beam size of 14 arcsec × 13 arcsec. The isophote defining the stellar disc (similarly to Fig. 2) is outlined by the black contour.
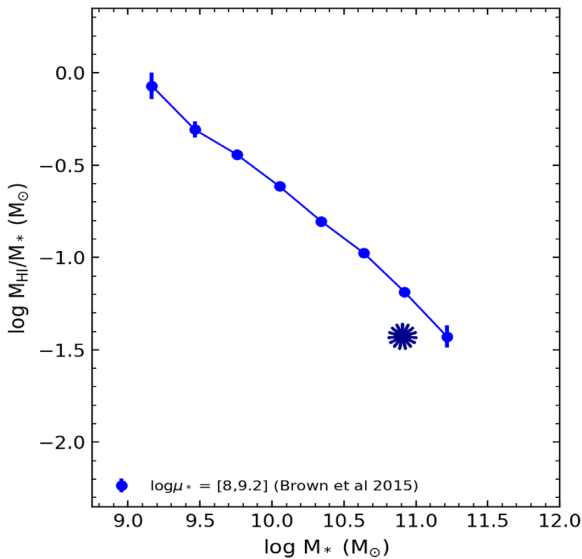
Figure 4. The average stacked H I fraction as a function of the stellar mass (Brown et al. 2015). In blue we show the relation separated into galaxies with stellar surface brightness comparable to that of JO206 within a factor of 4; the error bars represent the scatter in the mass bins. JO206 is illustrated by the blue asterisk.

the same mass (i.e. how much H I is in the tail). To do so we model the H I distribution assuming no ram-pressure stripping is affecting the galaxy and that all of its observed H I content is intact.

The model is based on the well-established and tight correlation that exists between H I masses and diameters of galaxies, and the self-similarity of the H I radial profiles (Broeils & Rhee 1997; Verheijen & Sancisi 2001; Noordermeer et al. 2005; Begum et al. 2008; Martinsson et al. 2016; Wang et al. 2016).

We use the H I size–mass relation parametrized by Wang et al. (2016) as

$$\log(D_{HI}/kpc) = 0.51 \log(M_{HI}/M_\odot) - 3.32, \tag{4}$$

where the H I diameter, D_{HI}, is defined at the H I surface density of 1 $M_\odot$ pc^{-2} ($N_{HI} = 1.25 \times 10^{20}$ atoms cm^{-2}). The observed scatter about this relation is 0.06 dex.

Based on this relation we calculate an H I diameter of $D_{HI} = 33$ kpc for the unperturbed JO206 model. The radial H I surface density distribution was determined using the Martinsson et al. (2016) H I profile formulated as

$$\Sigma_{HI}(R) = \Sigma_{HI}^{max} e^{\frac{-(R-R_{\Sigma,max})^2}{2\sigma_\Sigma^2}}. \tag{5}$$

In this equation the parameters $R_{\Sigma, max}$ and σ_Σ are fixed to the values $0.2 D_{HI}$ and $0.18 D_{HI}$, respectively (Martinsson et al. 2016). The only free parameter is Σ_{HI}^{max}, which we set to 0.4 $M_\odot pc^{-2}$ such that $\Sigma_{HI}(D_{HI}/2) = 1$ $M_\odot pc^{-2}$.

With the above-mentioned tools, and assuming the observational conditions described in Section 3, we modelled the unperturbed H I distribution of JO206 using the 3D-BAROLO package (Di Teodoro & Fraternali 2015). We used the position angle and inclination of the stellar disc as the inputs for model. The model was convolved with the H I beam within 3D-BAROLO. The resulting moment-0 map with the radial H I surface density profile is shown in the top panel of Fig. 5. The slight misalignment between the H I model and stellar disc is attributed to the effect of beam smearing by the H I beam which dominates this model.

The red ellipse in the figure outlines the model H I disc with a radius, $R_{HI} = 28$ kpc as defined at the H I column density sensitivity of 3×10^{19} atoms cm^{-2}. This corresponds to the sensitivity of our VLA observations and to the lowest H I contour shown for JO206 in Fig. 3. The model H I outside the red contour would not have been detected by our VLA observations and is therefore not considered

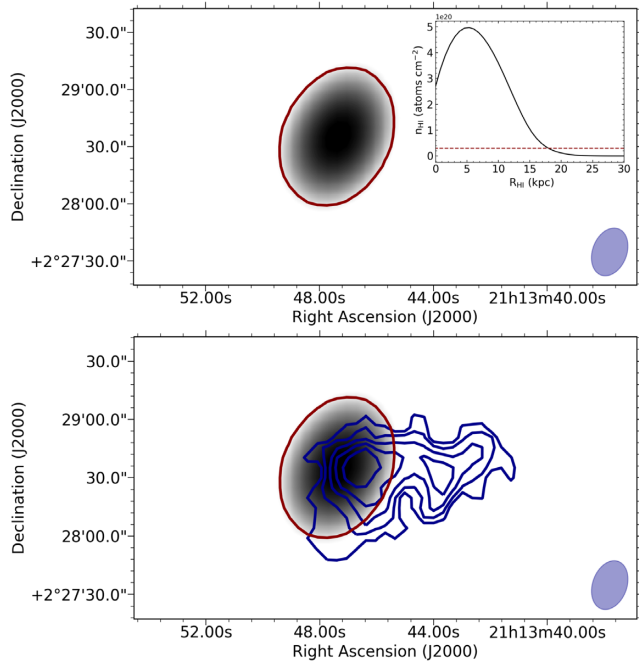**Figure 5.** The top panel shows the simulated H I distribution. The red contour is drawn at a column density of 3×10^{19} atoms cm^{-2}, the same as the lowest H I contour in our data. The red ellipse has a semimajor axis of 28 kpc. In the inset panel we show the model input H I radial profile with the red horizontal line indicating our sensitivity limit. In the bottom panel we compare the model H I with the observed distribution (blue contours). The observed H I column density levels are $n_{HI} = 3, 6, 9, ... \times 10^{19}$ atoms cm^{-2}. The FWHM beam size of 26 arcsec $\times$ 18 arcsec is indicated by the blue ellipse.

here. We compared the model and observed moment-0 maps as shown in bottom panel of Fig. 5. Any H I emission in the observed map that lies outside of the red contour should not be there and is considered the H I tail. Within this tail the measured H I mass is 1.8×10^9 M$_\odot$, which is ~60 per cent of the total H I mass in JO206.

We also determined how much of the total H I mass has simply been displaced relative to the model, regardless of whether it is inside or outside the 3×10^{19} atoms cm^{-2} model isophote in Fig. 5. This is calculated as H I$_{disp} = \Sigma |$mod$_{i,j} -$ obs$_{i,j}|/2$, where mod is the modelled H I, obs is the observed, and the indices i, j run through all pixels in the image. Using this formulation we find that an H I mass of 2.0×10^9 M$_\odot$ has been displaced relative to the model with about half of the signal found in the tail and the other half in the disc.

5 GAS AND STAR FORMATION ACTIVITY

We have determined that JO206 has lost about half of its neutral gas due to ram pressure by the ICM, and that 60 per cent of its remaining H I content is distributed along the 90 kpc-long tail of stripped gas. In this section we study the galaxy's star formation efficiency (SFE) under these stripping conditions by examining the relation between H I content and SFR. Given the known correlation between SFR and stellar mass (e.g. Brinchmann et al. 2004; Salim et al. 2007) we start by selecting a sample of galaxies with the same stellar mass as JO206. To do so we extracted all galaxies in the GALEX Arecibo SDSS Survey (GASS; Catinella et al. 2010) with a stellar mass within a factor of 4 of that of JO206. Then since SFR scales with H I mass at a fixed stellar mass (Doyle & Drinkwater 2006; Huang et al. 2012; Saintonge et al. 2016), we
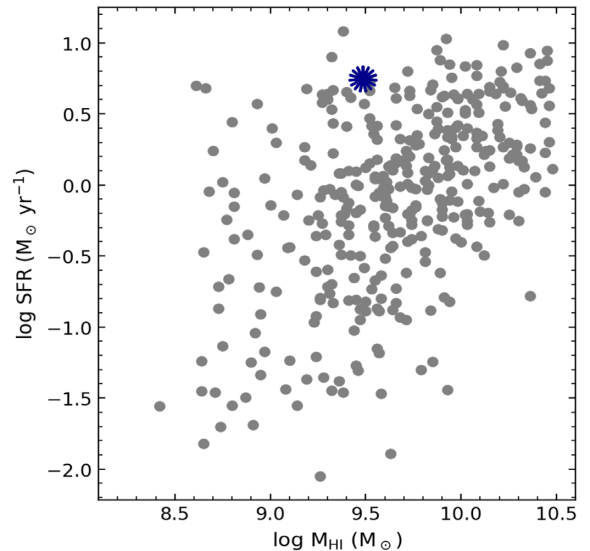

Figure 6. The SFR as a function of H I mass for galaxies with the same stellar masses as JO206. The grey points are galaxies from the GASS and the blue asterisk represents the JO206 galaxy.

plot SFR versus H I mass for this control sample in Fig. 6. We find that in comparison JO206 (SFR $= 5.6$ M$_\odot$ yr^{-1}) is about 0.5 dex above the general galaxy population implying that it is forming more stars than similar galaxies given its H I mass. The H I–SFR scaling relation has a large scatter, as shown in the aforementioned papers and in Fig. 6. Therefore, the exact SFR enhancement has large uncertainties. However, the fact that JO206 lies at the very edge of the observed distribution of our comparison sample is a relatively strong indication that some SFR enhancement has occurred. We calculate an overall H I gas depletion time-scale as $\tau_d = M_{HI}/$SFR, and find that it is 0.54 Gyr. This time-scale is shorter than that of a typical normal disc galaxy (~2 Gyr; Leroy et al. 2008). This indicates that the SFR is enhanced in this object compared to other galaxies with similar stellar and H I masses. The total SFR measured for JO206 would be more typical for a galaxy with the same stellar mass and an H I mass of approximately 3×10^{10} M$_\odot$, an order of magnitude above the measured M_{HI} of this galaxy.

5.1 Comparing H α to H I

To understand the reason for the higher than expected star formation activity of JO206 we use H α map (dust- and absorption-corrected) as a tracer for recent star formation. We compare its distribution with that of H I as shown in Fig. 7. The H I emission overlaps almost entirely with H α. The disagreement seen is due to the different spatial resolutions between the H I and H α data. We demonstrate this in Fig. 8 by comparing H I and H α surface brightness distribution along an arbitrary axis line (solid green line in Fig. 7) both before and after convolving the H α image with the H I PSF. Fig. 8 shows that H α emission is found at all positions with H I emission after convolution.

The H I map exhibits two local maxima where it peaks at H I column densities of ~1.6×10^{20} atom cm^{-2}. One is within the galaxy disc while the other is located at ~60 kpc from the galaxy centre in the middle of the tail. These bright H I regions coincide with areas with several knots of H α emission. These are regions at which we expect recent star formation. However, in the southern pointing (see Appendix A, Fig. A1) the H I is much more extended
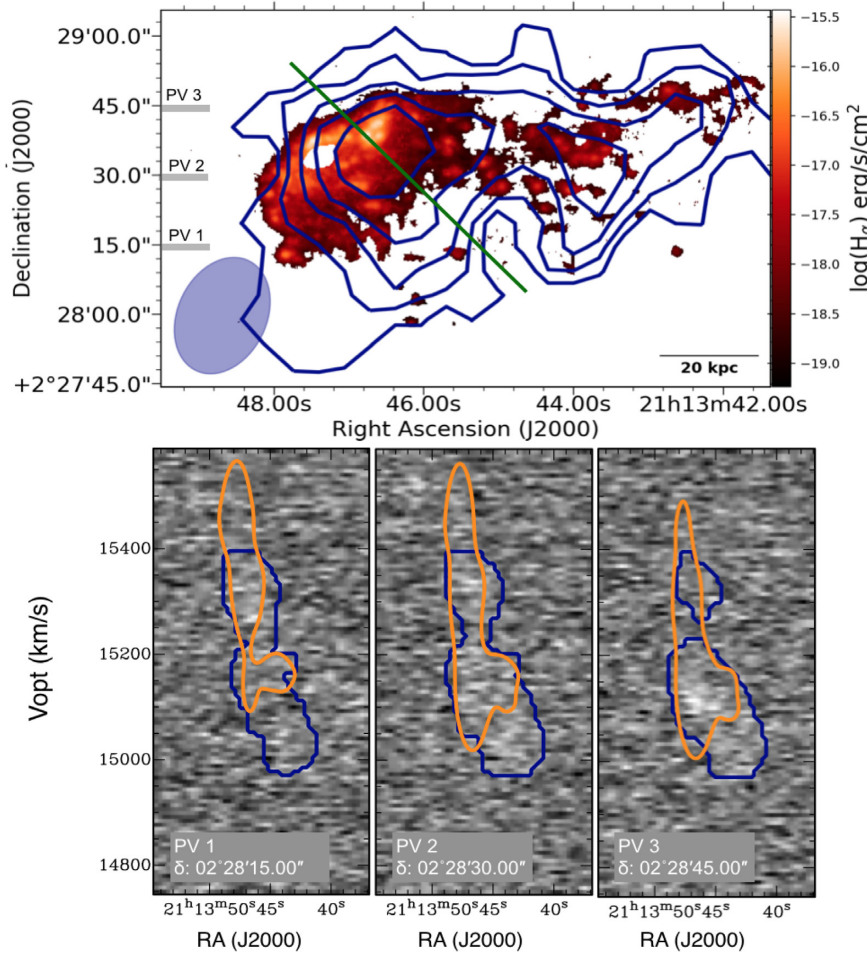
Figure 7. A comparison of the H I column density distribution with Hα map from MUSE. In the top panel the MUSE Hα is shown in red with the H I distribution overlaid in blue at column densities of 3, 6, 9, ... $\times 10^{19}$ atoms cm^{-2}. The green diagonal line indicates the slit position for the profile in Fig. 8. The bottom panel shows position velocity diagrams (PVDs) extracted along three declination slices (PV1, PV2, and PV3) in the H I cube. Velocities in the PVDs are in the optical definition using the barycentric standard of rest. The Hα emission convolved with the H I PSF is illustrated in orange and the underlying H I mask in the image cube is outlined by the blue contours.
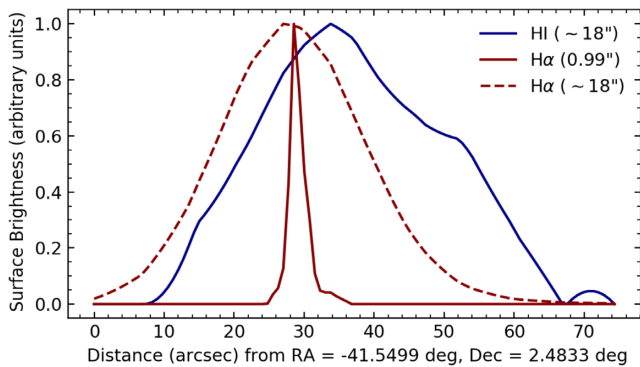
Figure 8. Comparison profiles along the diagonal line in Fig. 7. The red solid line represents the full resolution ($\sim$0.99 arcsec) Hα profile and the red dashed line is the Hα profile convolved with the H I PSF ($\sim$18 arcsec). Shown in blue is the H I line emission. The y-axis has arbitrary units and the x-axis is the distance in arcsec from the starting point (RA $= -41.5499$ deg, Dec. $= 2.4833$ deg) of the line from which the profile was extracted (i.e. the green diagonal line in Fig. 7).

than the Hα knots but it is at such low column densities that no star formation is expected in those regions.

The comparison between the Hα and H I PVDs in the bottom panel of Fig. 7 shows a general close agreement in the kinematics as well. However, the Hα appears to have a slightly higher velocity than the H I. This is due to the presence of Hα but not of H I (at the same angular resolution) in the eastern edge of the galaxy disc, which has receding velocity compared to systemic (see figs 6 and 7 in Poggianti et al. 2017b). The agreement between the velocities of cold H I gas and Hα, particularly along the tail is attributed to the ionization of the stripped gas by newly forming stars.

5.2 Star formation density and H I

To pinpoint where the observed enhanced star formation activity is taking place in JO206 we examine its SFR in relation to the H I gas density distribution. We start globally by comparing the SFR density map and the H I distribution in Fig. 9.

The map excludes Hα emission from the AGN. It shows an increased SFR within the disc in the western region around 40 kpc from the centre of the disc. This coincides with the location of the bright H I emission where CO has also been detected (see Fig. 2;
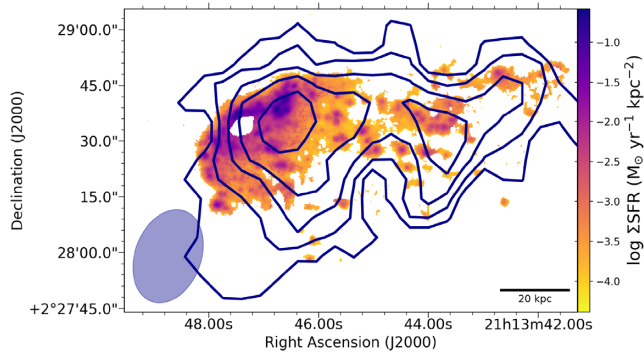
Figure 9. The SFR surface density map with the H I contour levels at the same levels as in Fig. 3. The white patch is the location of the excluded central AGN.

also Moretti et al. 2018). Further west in the tail there is continued star formation activity spread out in various regions with a star-forming knot around 60 kpc from the centre again corresponding with where the H I emission peaks. The APEX observation here can only provide an upper limit of 6.3×10^8 $M_\odot$ of molecular gas (Moretti et al. 2018).

The comparison shown in Fig. 9 however only offers a qualitative assessment of the SFR and gas correlations. It gave us clues to where the galaxy is likely forming stars with high efficiency.

We take this investigation further by studying this correlation in a spatially resolved way. This approach allows for improved statistics to pinpoint exactly where in the galaxy (disc or tail), gas forms stars efficiently. The effectiveness of this approach was illustrated by Bigiel et al. (2008) and Bigiel et al. (2010) who found a higher SFE in the inner regions of 'normal' field spiral galaxies compared to the outer parts, the latter being more likely dominated by H I. Boissier et al. (2012) also applied this approach to study SFE of a sample of galaxies that are possibly experiencing ram-pressure gas stripping in the Virgo cluster. They found that SFR was lower by an order of magnitude in the gas-stripped tails than within the galaxy.

To make a direct comparison between the star formation and H I map, we convolved the star formation surface density map (Fig. 9) with the H I beam and regridded to the same pixel scale of 5 arcsec. During this process the flux in the star formation surface density map was conserved. We then flagged pixels as being in the tail or disc based on whether they are inside or outside the H I model's 3×10^{19} atoms cm^{-2} contour (see Section 4.3) and performed a pixel-by-pixel analysis similar to the aforementioned studies.

As a control sample we use 'normal' field galaxies based on The H I Nearby Galaxy Survey (THINGS; Bigiel et al. 2008; Bigiel et al. 2010). Although SFR surface density maps of the control sample are based on a combination of FUV and 24 μm emission, a good agreement was shown with the Hα emission for this sample (see fig. 4 in Bigiel et al. 2008). This makes this sample suitable to compare with our measurements. Image maps in this control sample have a 750 pc spatial resolution. To enable a direct comparison with JO206 measurements we convolved these images to the same physical resolution as JO206 using a circular PSF with the same area as our 26 arcsec × 18 arcsec H I beam which is ∼22 kpc at the distance of JO206. We then only selected a control subsample of five galaxies which remained sufficiently resolved after this convolution, namely NGC 5055, NGC 2841, NGC 7331, NGC 3198, and NGC 3521.

Fig. 10 shows the resolved SFR surface density versus H I surface density within the disc (red) and in the tail (blue) of JO206. This is
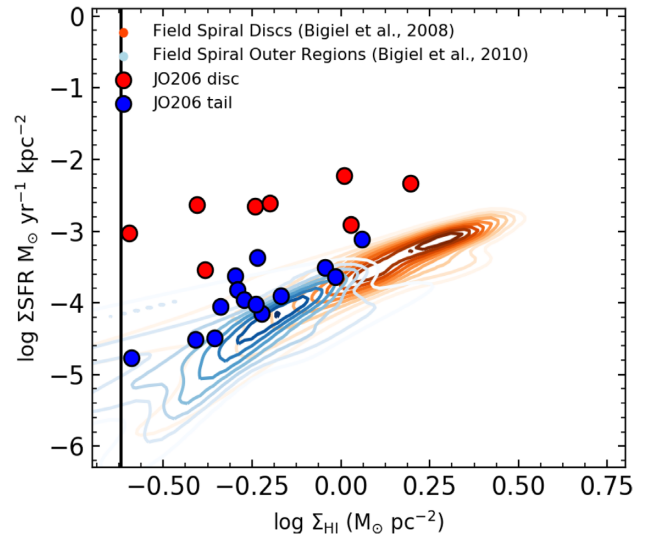

Figure 10. Relation between the SFR density and H I surface density. The red and blue points represent the main galaxy body and tail of JO206, respectively. These are plotted independently per beam. The orange density contours are the inner regions (discs) of field spiral galaxies selected from the THINGS sample from Bigiel et al. (2008) convolved with the H I beam. The light blue density contours represent the outer regions of spiral galaxies in the field (Bigiel et al. 2010) also convolved with the the H I beam. Contrary to the high-resolution map, THINGS galaxies form a single sequence. The solid vertical line indicates our H I sensitivity limit.
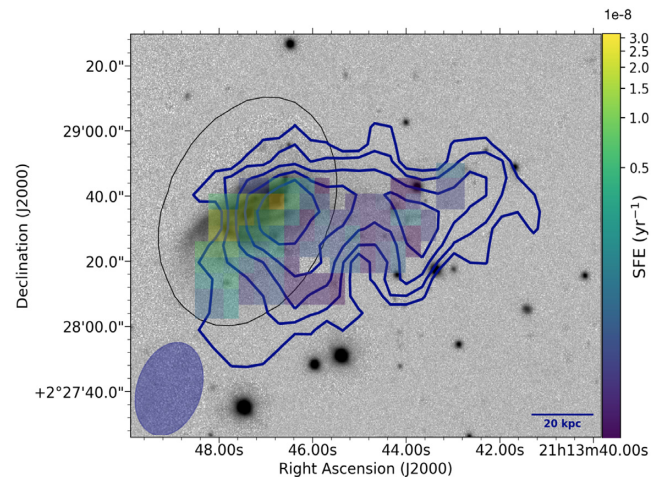

Figure 11. The SFE map with the colour bar indicating SFE values for pixels with SFE $\geq 10^{-9}$ yr^{-1}. The map is overlaid over the optical V-band image of JO206 and its H I distribution. H I column densities are $n_{\rm H I} = 3$, 6, 9, ... × 10^{19} atoms cm^{-2}. Outlined in black is the H I disc defined at the H I model's 3×10^{19} atoms cm^{-2} contour.

compared with the inner and outer regions of the THINGS control subsample smoothed to our resolution as described above. We find that the inner parts of JO206 are producing stars at a relatively higher rate than the outer regions at a given H I surface density. The SFR is about 10 times higher on average in the inner parts of the galaxy than the outer regions. This is not surprising since the stripped H I is less dense in the tail compared to the disc. However, both the inner and outer pixels of JO206 show higher SFRs for a given H I surface density compared to normal field galaxies in the control sample.

In total we measure an average total SFE (measured as SFR/M_{HI}) of $\sim 2 \times 10^{-9}$ yr^{-1} which is about a factor of 5 times higher than normal field local galaxies (Leroy et al. 2008; Schiminovich et al. 2010). We show in Fig. 11 the locations at which the JO206 is most efficient (SFE $\geq 10^{-9}$ yr^{-1}) at forming stars. Note that some correlation between adjacent pixels in the SFE map is present.

The observed enhanced star formation activity in the disc and especially the tail of JO206 persists even when compared to other ram-pressured gas-stripped galaxies in the Virgo cluster (see fig. 3 by Boissier et al. 2012). This could be because JO206 is a much more extreme case of ram-pressure stripping based on the extreme length of the observed tail. Furthermore, this spatially resolved result confirms the more global results of enhanced star formation activity in JO206 based on just H I mass and SFRs values (see Fig. 6).

6 SUMMARY

As part of the ESO MUSE GASP survey we have studied the H I gas phase of the prototypical 'jellyfish' galaxy in the sample, namely, JO206 (Poggianti et al. 2017b). This massive galaxy (M_* $\sim 8.5 \times 10^{10}$ M$_\odot$) resides in a poor cluster but exhibits a long Hα tail caused by ram-pressure stripping. In this paper we primarily focused on the stripping of H I and on the star formation activity associated with its H I content using data obtained with the VLA telescope. Our finding are as follows:

(i) As the result of ram-pressure stripping, we find that the H I distribution is perturbed and exhibits a one-sided, ~ 90 kpc H I tail from the optical disc. We measure a total H I mass of $M_{HI} = 3.2 \times 10^9$ M$_\odot$ of which 60 per cent (1.8×10^9 M$_\odot$) is in the gas-stripped tail. Overall the galaxy is about 50 per cent H I deficient. The observed stripped fraction of H I gas is consistent with estimations of gas mass lost from modelling of the cluster's ram-pressure and the galaxy's restoring force.

(ii) An assessment of the H I and SFRs shows that the galaxy is generally undergoing an enhanced star formation activity compared to its counterpart with the same stellar mass. The H I depletion time is ~ 0.5 Gyr in this galaxy which is shorter than that of 'normal' spiral galaxies in the field.

(iii) By comparing the H I distribution and the Hα distribution, we find a strong correlation between the observed cold gas and ionized emission (Hα). This is seen in both the galaxy main body and the tail. Moreover, the agreement persists in the kinematics of the galaxy. This indicates a strong link between the presence of cold gas and the recent star formation across all of the galaxy.

(iv) To pinpoint the exact locations at which the new stars are forming with high efficiency, we smoothed and regridded the MUSE SFRD maps to our H I resolution and pixel scale, and conducted a pixel-by-pixel analysis of the SFR density and the H I surface density. We tagged pixels belonging to the galaxy disc and tail. Our results show that the SFE in the disc is on average ~ 10 times higher compared to the tail for a given H I surface density. We find that in general the inner and outer parts of JO206 have relatively higher star formation efficiencies compared to galaxies in the literature (Bigiel et al. 2008; Bigiel et al. 2010), even compared to those undergoing ram-pressure stripping in the Virgo cluster (Boissier et al. 2012).

This work contributes to the ongoing efforts by the GASP survey in understanding the fate of gas in galaxies during the ram-pressure stripping phenomenon. We highlighted the importance of studying the H I gas phase and understanding the link between the gas and star formation activity of the JO206 galaxy as it falls into the cluster.

The GASP data showed that star formation in the gas-stripped tails is common in the sample. However, understanding particularly the formation of stars in the gas-stripped tails is not trivial and this is the case with JO206. There are a number of properties to be taken into account such as the environmental conditions. JO206 is special in this case because it is massive galaxy undergoing ram pressure in a rather poor galaxy cluster. Although a significant fraction (~ 60 per cent) of the H I has been displaced, it is still visible in the form of H I. i.e. it has not been immediately ionized by (or lost to) the ICM. In other words, at its current stripping stage, JO206 still has fuel to form new stars along its tail and disc. Comparing this galaxy with others in the GASP sample in different environments will clarify whether the environment played a pivotal role in the enhanced observed star formation or whether other specific physical conditions are responsible.

REFERENCES

Abadi M. G., Moore B., Bower R. G., 1999, MNRAS, 308, 947
Abramson A., Kenney J. D. P., Crowl H. H., Chung A., van Gorkom J. H., Vollmer B., Schiminovich D., 2011, AJ, 141, 164
Aguado D. S. et al., 2019, ApJS, 240, 23
Baldry I. K., Glazebrook K., Brinkmann J., Ivezić Ž., Lupton R. H., Nichol R. C., Szalay A. S., 2004, ApJ, 600, 681
Balogh M. L. et al., 2009, MNRAS, 398, 754
Begum A., Chengalur J. N., Karachentsev I. D., Sharina M. E., Kaisin S. S., 2008, MNRAS, 386, 1667
Bigiel F., Leroy A., Walter F., Brinks E., de Blok W. J. G., Madore B., Thornley M. D., 2008, AJ, 136, 2846
Bigiel F., Leroy A., Walter F., Blitz L., Brinks E., de Blok W. J. G., Madore B., 2010, AJ, 140, 1194
Biviano A. et al., 2017, A&A, 607, A81
Boissier S. et al., 2012, A&A, 545, A142
Boselli A. et al., 2016, A&A, 587, A68
Boselli A., Gavazzi G., 2006, PASP, 118, 517
Boulares A., Cox D. P., 1990, ApJ, 365, 544
Bravo-Alfaro H., Szomoru A., Cayatte V., Balkowski C., Sancisi R., 1997, A&AS, 126, 537
Bravo-Alfaro H., Cayatte V., van Gorkom J. H., Balkowski C., 2000, AJ, 119, 580

Brinchmann J., Charlot S., White S. D. M., Tremonti C., Kauffmann G., Heckman T., Brinkmann J., 2004, MNRAS, 351, 1151

Broeils A. H., Rhee M.-H., 1997, A&A, 324, 877

Brown T., Catinella B., Cortese L., Kilborn V., Haynes M. P., Giovanelli R., 2015, MNRAS, 452, 2479

Cardelli J. A., Clayton G. C., Mathis J. S., 1989, ApJ, 345, 245

Catinella B. et al., 2010, MNRAS, 403, 683

Catinella B. et al., 2018, MNRAS, 476, 875

Cattaneo A., 2015, Nature, 521, 164

Cava A. et al., 2009, A&A, 495, 707

Chabrier G., 2003, PASP, 115, 763

Chung A., van Gorkom J. H., Kenney J. D. P., Vollmer B., 2007, ApJ, 659, L115

Chung A., van Gorkom J. H., Kenney J. D. P., Crowl H., Vollmer B., 2009, AJ, 138, 1741

Cooper M. C. et al., 2007, MNRAS, 376, 1445

Cortese L., Gavazzi G., Boselli A., Franzetti P., Kennicutt R. C., O'Neil K., Sakai S., 2006, A&A, 453, 847

De Lucia G., 2011, in Ferreras I., Pasquali A., eds, Astrophysics and Space Science Proceedings, Vol. 27, Modelling the Evolution of Galaxies as a Function of Environment. Environment and the Formation of Galaxies: 30 years later. Springer-Verlag, Berlin, Heidelberg, p. 203

Dekel A., Birnboim Y., 2006, MNRAS, 368, 2

Di Teodoro E. M., Fraternali F., 2015, MNRAS, 451, 3021

Doyle M. T., Drinkwater M. J., 2006, MNRAS, 372, 977

Dressler A. et al., 1997, ApJ, 490, 577

Dressler A., 1980, ApJ, 236, 351

Dressler A., Oemler A. Jr, Poggianti B. M., Gladders M. D., Abramson L., Vulcani B., 2013, ApJ, 770, 62

Duc P.-A., Bournaud F., 2008, ApJ, 673, 787

Fabello S., Kauffmann G., Catinella B., Li C., Giovanelli R., Haynes M. P., 2012, MNRAS, 427, 2841

Fasano G. et al., 2006, A&A, 445, 805

Foltz R. et al., 2018, ApJ, 866, 136

Fossati M., Fumagalli M., Boselli A., Gavazzi G., Sun M., Wilman D. J., 2016, MNRAS, 455, 2028

Fumagalli M., Fossati M., Hau G. K. T., Gavazzi G., Bower R., Sun M., Boselli A., 2014, MNRAS, 445, 4335

Gavazzi G. et al., 2008, A&A, 482, 43

Gavazzi G., Contursi A., Carrasco L., Boselli A., Kennicutt R., Scodeggio M., Jaffe W., 1995, A&A, 304, 325

George M. R. et al., 2011, ApJ, 742, 125

Gullieuszik M. et al., 2015, A&A, 581, A41

Gullieuszik M. et al., 2017, ApJ, 846, 27

Gunn J. E., Gott J. R. III, 1972, ApJ, 176, 1

Güsten R., Nyman L. Å., Schilke P., Menten K., Cesarsky C., Booth R., 2006, A&A, 454, L13

Haynes M. P., Giovanelli R., Chincarini G. L., 1984, ARA&A, 22, 445

Huang S., Haynes M. P., Giovanelli R., Brinchmann J., 2012, ApJ, 756, 113

Jáchym P., Palouš J., Köppen J., Combes F., 2007, A&A, 472, 5

Jáchym P., Köppen J., Palouš J., Combes F., 2009, A&A, 500, 693

Jaffé Y. L. et al., 2016, MNRAS, 461, 1202

Jaffe Y. L. et al., 2018, MNRAS, 476, 4753

Jaffé Y. L., Smith R., Candlish G. N., Poggianti B. M., Sheen Y.-K., Verheijen M. A. W., 2015, MNRAS, 448, 1715

Kapferer W., Sluka C., Schindler S., Ferrari C., Ziegler B., 2009, A&A, 499, 87

Kenney J. D. P., Tal T., Crowl H. H., Feldmeier J., Jacoby G. H., 2008, ApJ, 687, L69

King A., Pounds K., 2015, ARA&A, 53, 115

Kronberger T., Kapferer W., Ferrari C., Unterguggenberger S., Schindler S., 2008, A&A, 481, 337

Larson R. B., 1972, Nature, 236, 21

Leroy A. K., Walter F., Brinks E., Bigiel F., de Blok W. J. G., Madore B., Thornley M. D., 2008, AJ, 136, 2782

Madau P., Dickinson M., 2014, ARA&A, 52, 415

Martinsson T. P. K., Verheijen M. A. W., Bershady M. A., Westfall K. B., Andersen D. R., Swaters R. A., 2016, A&A, 585, A99

McMullin J. P., Waters B., Schiebel D., Young W., Golap K., 2007, in Shaw R. A., Hill F., Bell D. J., eds, ASP Conf. Ser. Vol. 376, Astronomical Data Analysis Software and Systems XVI. Astron. Soc. Pac., San Francisco, p. 127

Merluzzi P. et al., 2013, MNRAS, 429, 1747

Merluzzi P., Busarello G., Dopita M. A., Haines C. P., Steinhauser D., Bourdin H., Mazzotta P., 2016, MNRAS, 460, 3345

Moore B., Katz N., Lake G., Dressler A., Oemler A., 1996, Nature, 379, 613

Moran S. M., Ellis R. S., Treu T., Smith G. P., Rich R. M., Smail I., 2007, ApJ, 671, 1503

Moretti A. et al., 2014, A&A, 564, A138

Moretti A. et al., 2017, A&A, 599, A81

Moretti A. et al., 2018, MNRAS, 475, 4055

Nantais J. B. et al., 2017, MNRAS, 465, L104

Noeske K. G. et al., 2007, ApJ, 660, L43

Noordermeer E., van der Hulst J. M., Sancisi R., Swaters R. A., van Albada T. S., 2005, A&A, 442, 137

Offringa A. R. et al., 2014, MNRAS, 444, 606

Offringa A. R., de Bruyn A. G., Biehl M., Zaroubi S., Bernardi G., Pandey V. N., 2010, MNRAS, 405, 155

Peng Y., Maiolino R., Cochrane R., 2015, Nature, 521, 192

Perley R. et al., 2009, Proceedings of IEEE, 97, 1448

Poggianti B. M. et al., 2016, AJ, 151, 78

Poggianti B. M. et al., 2017a, Nature, 548, 304

Poggianti B. M. et al., 2017b, ApJ, 844, 48

Porter S. C., Raychaudhury S., Pimbblet K. A., Drinkwater M. J., 2008, MNRAS, 388, 1152

Postman M. et al., 2005, ApJ, 623, 721

Quilis V., Moore B., Bower R., 2000, Science, 288, 1617

Reiprich T. H., 2001, PhD thesis, Max-Planck-Institut für extraterrestrische Physik

Roediger E., Brüggen M., 2006, MNRAS, 369, 567

Roediger E., Brüggen M., 2007, MNRAS, 380, 1399

Roediger E., Brüggen M., 2008, MNRAS, 388, 465

Roediger E., Hensler G., 2005, A&A, 433, 875

Saintonge A. et al., 2016, MNRAS, 462, 1749

Salim S. et al., 2007, ApJS, 173, 267

Schiminovich D. et al., 2010, MNRAS, 408, 919

Schulz S., Struck C., 2001, MNRAS, 328, 185

Serra P. et al., 2015, MNRAS, 448, 1922

Silk J., Mamon G. A., 2012, Res. Astron. Astrophys., 12, 917

Skrutskie M. F. et al., 2006, AJ, 131, 1163

Smith R. et al., 2015, MNRAS, 454, 2502

Smith R. J. et al., 2004, AJ, 128, 1558

Smith R. J. et al., 2010, MNRAS, 408, 1417

Smith G. P., Treu T., Ellis R. S., Moran S. M., Dressler A., 2005, ApJ, 620, 78

Sun M., Vikhlinin A., 2005, ApJ, 621, 718

Sun M., Donahue M., Voit G. M., 2007, ApJ, 671, 190

Sun M., Donahue M., Roediger E., Nulsen P. E. J., Voit G. M., Sarazin C., Forman W., Jones C., 2010, ApJ, 708, 946

Tonnesen S., Bryan G. L., 2009, ApJ, 694, 789

Tonnesen S., Bryan G. L., 2010, ApJ, 709, 1203

Toomre A., Toomre J., 1972, ApJ, 178, 623

Valentinuzzi T. et al., 2009, A&A, 501, 851

van der Wel A. et al., 2014, ApJ, 788, 28

Varela J. et al., 2009, A&A, 497, 667

Verheijen M. A. W., Sancisi R., 2001, A&A, 370, 765

Vollmer B. et al., 2012, A&A, 537, A143

Vollmer B., 2003, A&A, 398, 525

Vollmer B., 2009, A&A, 502, 427

Vollmer B., Cayatte V., Balkowski C., Duschl W. J., 2001, ApJ, 561, 708

Vollmer B., Beck R., Kenney J. D. P., van Gorkom J. H., 2004, AJ, 127, 3375

Vollmer B., Huchtmeier W., van Driel W., 2005, A&A, 439, 921

Vollmer B., Soida M., Otmianowska-Mazur K., Kenney J. D. P., van Gorkom J. H., Beck R., 2006, A&A, 453, 883

Vollmer B., Braine J., Pappalardo C., Hily-Blant P., 2008, A&A, 491, 455

Walker I. R., Mihos J. C., Hernquist L., 1996, ApJ, 460, 121

Walter F., Brinks E., de Blok W. J. G., Bigiel F., Kennicutt Jr. R. C., Thornley M. D., Leroy A., 2008, AJ, 136, 2563

Wang J., Koribalski B. S., Serra P., van der Hulst T., Roychowdhury S., Kamphuis P., Chengalur J. N., 2016, MNRAS, 460, 2143

Whitaker K. E., Kriek M., van Dokkum P. G., Bezanson R., Brammer G., Franx M., Labbé I., 2012, ApJ, 745, 179

White S. D. M., Frenk C. S., 1991, ApJ, 379, 52

Yagi M. et al., 2010, AJ, 140, 1814

Yagi M., Komiyama Y., Yoshida M., Furusawa H., Kashikawa N., Koyama Y., Okamura S., 2007, ApJ, 660, 1209

Yoon H., Chung A., Smith R., Jaffé Y. L., 2017, ApJ, 838, 81

APPENDIX: SUPPLEMENTARY MUSE OBSERVATIONS

VLA observations detected H ı emission outside the region covered by the initial GASP observations with MUSE presented in GASP I (Poggianti et al. 2017b), as shown in Fig. 3. To check for possible H α emission in the southern tail of the H ı emission we obtained new MUSE observations. These were carried out as part of ESO programme 0102.C-0589, a filler program designed to use idle time at the VLT UT4 during the worst weather conditions. Observations were carried out under non-photometric conditions between 2018 October 3 and 2018 October 6; we obtained 16×900 s exposures of a single MUSE pointing. The total exposure time of 4 h is much larger than the one of normal GASP observations (2700 s) to compensate for possible loss due to the bad weather conditions.

Observations were carried out under thin and thick cirrus and seeing between 1.3 and 0.6 arcsec (as measured by the DIMM). The new MUSE data were reduced using the standard GASP data reduction procedure (see GASP I Poggianti et al. 2017b for details). Because the observations were carried out under non-optimal weather conditions, we corrected the fluxes by comparing the H α fluxes measured in the regions in common with the original GASP observations. We found that the fluxes obtained from the new observations are 1.66 times lower than those obtained from the
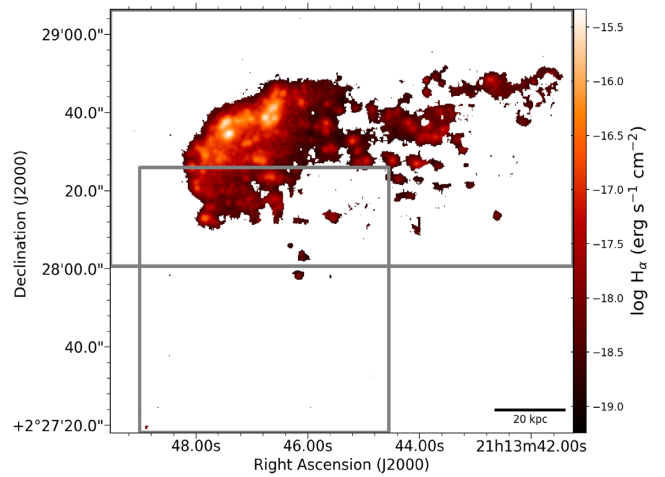

Figure A1. The MUSE H α map with the old and new MUSE FoV pointings overlaid are outlined in grey. The new pointing to the south of the map.

original GASP data. We therefore rescaled the data cube obtained from the new observations by this factor to put all observations on the same flux scale.

The combined H α emission map is shown in Fig. A1 together with the FoV of the new MUSE observations and of the original GASP ones. We compared the r.m.s. of the background and the distribution of the measured H α fluxes in the overlapping regions and we conclude that the new observations are at least as deep as the original GASP ones. The new observations revealed three new H α blobs beyond the region covered by the original GASP observations. An analysis of the BPT diagram indicates that the gas in these three regions is ionized by young stars.

This paper has been typeset from a TEX/LATEX file prepared by the author.